Pure & Appl. Chem., Vol. 65, No. 2, pp. 285–295, 1993.
Printed in Great Britain.

The mass spectrometric sampling of ions from atmospheric pressure flames as exemplified by the reactions of OH^- and O_2^- in O_2-rich flames

A.N. Hayhurst

Department of Chemical Engineering, Cambridge University, Pembroke Street, Cambridge CB2 3RA, U.K.

Abstract - A description of an apparatus to continuously extract ions from a flame and subject them to mass spectroscopic analysis is given. The measured ion concentrations can be falsified, because of fast reactions shifting whilst the sample enters the vacuum chamber of the mass spectrometer. In addition, free electrons can diffuse to the metallic sampling cone. These problems are exemplified by observations of OH^- and O_2^- in an O_2-rich flame. Interestingly the fast reactions undergone by OH^- and O_2^- lead to quasi-steady-state concentrations of these ions in such a flame.

INTRODUCTION

Mass spectrometry has been used now for many years to identify the species present in a flame. The flame can be at or below atmospheric pressure; also the species under study can be stable or transient, *e.g.* a radical or an electrically charged ion. In any case a sample of the flame has to be taken continuously and reduced to a pressure low enough for mass spectrometry *i.e.* below around 10^{-5} mbar. The work reported here is mainly concerned with the mass spectrometry of ions present in a flame at atmospheric pressure. Many of the problems of such a study also arise in the investigation of *e.g.* neutral molecules or free radicals in any reacting system. We accordingly begin with a description of one apparatus and then discuss the difficulties of such a study. Some of these problems have been outlined before.[1,2]

EXPERIMENTAL

Fig. 1 shows the burner, on which sits a steady flame. In this work the flame was mainly a fuel-lean, premixed flame of $H_2 + O_2 + N_2$; the unburnt gas had molar ratios of $H_2/O_2/N_2 = 1.50/1.00/3.55$. The burner comprised a bundle of 150 stainless steel, hypodermic, tubes of internal diameter 0.6 mm. The gases flowing through each tube produced a visible reaction zone extending some 1.5 mm from the flat burner face. Afterwards the burnt gases extended some 50 mm from the burner, *i.e.* until entrainment of air both cooled and altered the composition of the hot mixture, principally of H_2O, O_2 and N_2. The temperature on the axis of this flame was measured[3] by the Na-D line reversal technique to be about 1400 K just downstream of the reaction zone; subsequently the temperature rises (because of radical recombination[3]) to 2070 K at 15 mm from the burner face. Thereafter it was steady at this value, which is 75 K less than the calculated adiabatic temperature of 2145 K. It will be seen below that there is a region of the burnt gases which is not affected by air-entrainment. The axial velocity of the gases is fairly constant in this region and is equal to 13 m/s. This corresponds to laminar, plug flow. There are negligible radial velocities. Metal salts were added to a flame by nebulising *e.g.* an aqueous solution of KOH into the burner supplies. This procedure provides free K atoms, KOH molecules and K^+ ions, as well as free electrons.

Fig. 1 shows the flame burning against a water-cooled plate containing the sampling nozzle at its centre. This hollow, conical nozzle had walls 0.2 mm thick at an angle of 30° to the horizontal axis of the system.

The nozzle was electro-formed from nickel and had a circular hole at its apex. The diameter of this inlet orifice was in the range 60-210 μm. Gas passed continuously through the hole into the first vacuum chamber, which was evacuated to ≈ 10^{-3} mbar by a large oil diffusion pump. On entering the sampling nozzle, the temperature, pressure and concentrations of each species all fall rapidly. The ideal is for every reaction to stop instantaneously, so that relative concentrations do not change during sampling. This is discussed further below. Fig. 1 also shows the cylindrical first electrode. Imagine that positive ions are under investigation. In this case a voltage of about -15 V (with respect to the earthed front plate) on the first electrode accelerates positive ions, but rejects negatively charged ones. Thus a beam of positive ions and neutral species enters the second chamber, differentially pumped to almost 10^{-6} mbar. This chamber houses a quadrupole mass spectrometer, into which the beam of positive ions is directed and focussed. The ions of selected mass emerge from the spectrometer, are collected in a Faraday cup and their current is measured with a very sensitive d.c. amplifier. Negative ions can be observed by simply reversing the polarity of every accelerating potential. Sampling is normally along the axis of a flame and is achieved by moving the burner horizontally.

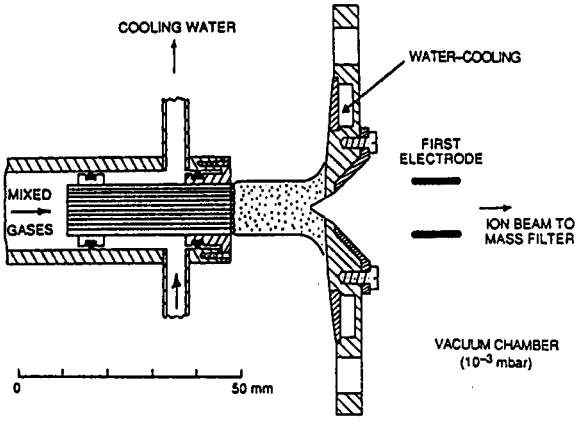

Fig. 1. Vertical cross-section through the burner, the flame, the water-cooled front plate with the sampling nozzle and the ring electrode inside the first vacuum chamber.

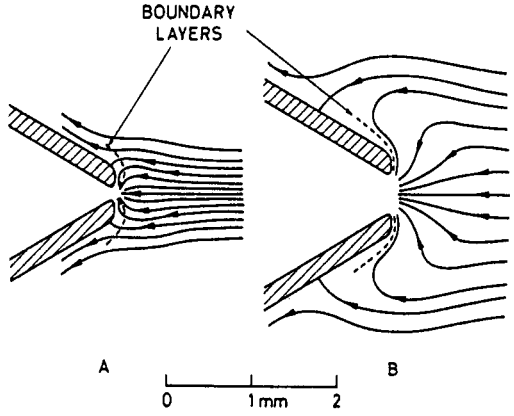

Fig. 2. Sketch of the flow field near the tip of a sampling cone for a relatively small orifice (A) and a large one (B). The thickness of the boundary layers and the locations of the streamlines are not precise.

SAMPLING CONSIDERATIONS

Consider now the flow of gas from the flame, through the inlet hole and down the conical expansion duct (see fig. 2) into the first vacuum chamber. Because the ratio of the pressures in the flame and in the first vacuum chamber exceeds[4] the value of 2, or more exactly

$$\left(\frac{1+\gamma}{2}\right)^{\gamma/(\gamma-1)}$$

where γ (≈ 1.3) is the ratio of the principal specific heats of the gaseous sample, the flow at the narrower part of the inlet orifice is choked. Thus, the local Mach number (the ratio of the flow velocity to the local velocity of sound, *i.e.* $(\gamma RT/M_w)^{1/2}$, where M_w is the mean molecular weight of the sampled gases) is unity[4] and the mass flow rate[4] into the vacuum chamber is

$$A_t p_o \left(\frac{\gamma M_w}{RT_f}\right)^{1/2} \left(\frac{2}{\gamma+1}\right)^{\frac{\gamma+1}{2(\gamma-1)}} \qquad \text{(I)}$$

Here A_t is the area of the throat, *i.e.* the narrowest part of the inlet hole, R is the gas constant and T_f is the temperature of the flame when undisturbed by sampling. After passing through the inlet orifice the gases expand adiabatically down the conical duct. The Mach number, M_a, exceeds unity and increases according to

$$\frac{A}{A_t} = \frac{1}{M_a}\left\{\frac{2}{1+\gamma}\left(1+\frac{(\gamma-1)}{2}M_a^2\right)\right\}^{\frac{\gamma+1}{2(\gamma-1)}}$$

for isentropic adiabatic flow. Here A is the cross-sectional area of the expansion duct. Whilst the Mach

number increases, the temperature, T, of the expanding gas sample falls and is given by

$$\frac{T_f}{T} = 1 + \frac{1}{2}(\gamma - 1) M_a^2 = \left(\frac{p_f}{p}\right)^{(\gamma - 1)/\gamma} \qquad \text{(II)}$$

Here p is the pressure at a point along the expansion and p_f is the stagnation pressure in the flame. Thus, when $M_a = 1$ at the throat of the orifice, $T/T_f = 0.88$ for $\gamma = 1.27$. Similarly the pressure at the entrance plane of the nozzle is 0.55 times that in the undisturbed flame. After the gases have moved a distance of one orifice diameter down the expansion duct, A/A_t becomes 4.64. If $\gamma = 1.27$, then $M_a = 2.85$ at this point, where $T/T_f = 0.48$ and the pressure has fallen to 0.032 times that in the flame. Thus the temperature, pressure and density fall rapidly in such an expansion. Ultimately collisions become unimportant when the local mean free path equals the diameter of the duct. This transition from continuum to molecular flow occurs at a distance of 6 nozzle diameters along the expansion for the smallest sampling hole (diam. = 60 μm), but at some 20 orifice diameters for the largest (210 μm). It is worthy of note that collisions do not cease at a particular dimensionless distance inside the sampling cone. Of course, chemical reactions do not usually occur at every collision, but they are able to proceed for longer times in a sampling system with a larger inlet orifice. In addition, the pressure of the flame has a large effect on the length of time for which reactions occur in the sampling nozzle.

Expression (I) gives the mass flow rate into an ideal nozzle. In practice the observed flow rate is often less than this by a factor called the discharge coefficient. Measurements of the flow rate of gases pumped out of the first vacuum indicate that in this present system the discharge coefficient is unity. This is higher than the previously[5] measured value of 0.62 with a flatter sampling plate, from which the sampling nozzle did not protrude as much as in Fig. 1.

The above considerations neglected any considerations of heat, mass or momentum transfer between the flame and the sampling nozzle. Even for this ideal case, the sample from the flame cools as it accelerates to higher velocities. This is seen from eq. (II), which shows that T_t, the temperature of the gases at the throat of the inlet hole becomes

$$T_t = T_f / \{1 + \tfrac{1}{2}(\gamma - 1)\}$$

This constitutes an inevitable 'aerodynamic' cooling and for the particular flame ($\gamma = 1.27$; $T_f = 2070$ K) under consideration amounts to a fall in temperature of 246 K. In addition, the gases entering the vacuum system are cooled by passing close to the water-cooled sampling nozzle, whose temperature can be measured by optical pyrometry to be around 900 K. In fact, the nickel nozzle is hottest when the flame is sampled close to its reaction zone. This is because the flame contains significant quantities (≤ 0.1 mole %) of the free radicals: H, OH and O, whose concentrations have maxima close to the reaction zone[3]. Clearly these radicals diffuse to the nickel nozzle, where they recombine, producing local heating. In any event the sampling cone is always kept deliberately cooler than the flame, because nickel melts at 1728 K. The contacting of the flame with the sampling nozzle is shown in Fig. 2, which in fact refers to a large and a small inlet orifice. In either case the flow is separated into two parts by a stagnation streamline. The first is that part of the flame which enters the sampling cone and thereby makes up the sample. Otherwise, the gases well away from the axis are not under observation, since they do not pass through the inlet hole. With a small orifice the gas sample moves relatively close to the nickel surface, but with a large inlet hole more of the sample is unaffected by the solid wall. A better way of expressing this is that a larger hole provides a stronger sink and "sucks in" more of the boundary layer. The outcome is that with a small inlet hole contact between the sample and nickel nozzle is more important than with a larger orifice, leading in turn to more 'boundary layer' cooling.

So far the sample has been seen to undergo cooling on the flame side of the sampling cone and also in the supersonic expansion within the conical expansion duct. The former is more important with small inlet orifices, the latter with large sampling holes. What is the effect of such cooling? Consider the pair of reactions:

$$Na^+ + H_2O + M \rightleftharpoons Na^+.H_2O + M \qquad \text{(III)}$$

where M is any flame molecule acting as a chaperone to remove the energy released when the first hydrate of Na^+ forms. It has been established[6] that the forward and backward steps in reaction (III) are fast

enough for it to be at equilibrium in a flame. In this case when a flame is sampled the temperature is reduced in two stages, *viz* on the high pressure side of the sampling nozzle and also in the adiabatic expansion inside the nickel cone. Reaction (III) is exothermic and so the effect of cooling on the gas sample is to create more $Na^+.H_2O$ by the equilibrium shifting position in the exothermic direction. Of course, there comes a point during sampling when such a shift stops and reaction (III) 'freezes'. This occurs when the time constant for scheme (III) becomes larger than the subsequent residence time in the sampling system before collisions cease. Such residence times can be calculated[7] for the adiabatic, supersonic expansion inside the sampling nozzle. In fact, as noted above they depend on γ, flame conditions and the diameter of inlet hole. However, for a nozzle of hole diameter 0.1 mm, with gas of mean molecular weight 20, γ of 1.26 and an initial temperature of 2000 K, the total residence time of the sample in the nickel cone before collisions cease is $\approx 2.5 \times 10^{-7}$ s. In this case any reaction with a time constant larger in magnitude cannot proceed to any significant extent in the adiabatic expansion. As an aside, these calculations[7] show that if the sampling cone has a half angle of 30°, the above one-dimensional description of the flow field within it is sufficiently accurate.

The mean residence time of the sample in the boundary layer before entering the sampling cone is difficult to compute. However, experimental studies[8] of the equilibrium:

$$HCl + e^- \rightleftharpoons Cl^- + H$$

with a wide range of sampling orifices show that the observed ratio $[Cl^-]/[e^-]$ is affected by cooling both before and after entering the vacuum system. Detailed examination of the measurements of $[Cl^-]/[e^-]$ indicate that for a nozzle diameter of around 0.05 mm the mean residence times of the sample in the boundary layer and supersonic expansion are roughly equal and close to 10^{-7} s. Also cooling in the external boundary layer becomes negligible[8] if the orifice diameter exceeds 0.15 mm. However, the 'aerodynamic' cooling noted earlier is inevitable. Thus for a reaction to be perturbed during sampling its time constant in the flame must be less than 10^{-6} s; also ΔH must be far from zero for an equilibrium to respond to changes in temperature. The first requirement of a small time constant ($< 10^{-6}$ s) means that the reaction must be equilibrated in the burnt gases, where the residence time is typically a few ms. Thus a reaction like

$$H + H + M \rightarrow H_2 + M$$

is too slow to be at equilibrium in a flame at atmospheric pressure and hence does not proceed during sampling. However, the reaction

$$OH + H_2 \rightleftharpoons H_2O + H \qquad \text{(IV)}$$

has $\Delta H = -63$ kJ/mol and in a fuel-rich flame of $H_2 + O_2 + N_2$ at 2000 K has a time constant of *ca* 1×10^{-7} s. Thus the reaction is equilibrated in the flame's reaction zone, where the residence time is ≈ 20 μs, as well as in the burnt gases. Also, it is likely that this equilibrium will be perturbed slightly during sampling. If the temperature falls from 2070 to 1770 K, then the equilibrium constant of reaction (IV) increases by a factor of 1.86. Generally speaking, reactions of ions are faster even than those of radicals; in addition, their values of ΔH can be larger. The overall result is that ionic reactions are often equilibrated in a flame and also shifted by the cooling brought about by sampling.

One difficulty is peculiar to the sampling of ions in a flame. If a potential difference $\Delta\phi$ is applied between the nozzle and the burner, the observed ion currents vary as shown in fig. 3. The two major positive ions, K^+ and H_3O^+, have maximum ion currents when $\Delta\phi$ is zero, but the principal negative ions, OH^- and HCO_3^- (actually two unresolved ions CO_3^- and HCO_3^-) have largest currents for positive $\Delta\phi$. This behaviour arises from the nickel cone acting as a Langmuir probe[9]. Free electrons are present and constitute the difference between the total concentrations of positive and negative ions in fig. 3. Because of their mobility free electrons can leave the flame sample, whilst it approaches the inlet orifice, and attach to the nickel surface. This leaves a sheath of positive ions in the flame gas adjacent to the sampling nozzle[9]. Thus when $\Delta\phi \approx 0$ positive ions experience an electrical field directing them towards the tip and walls of the sampling cone. A large, applied positive $\Delta\phi$ results in positive ions being repelled by the nickel surface, whereas, when $\Delta\phi$ is very negative, all the positive ions are attracted to the nickel surface.

Fig. 3 reflects how many ions pass through the inlet hole and it is probably fortuitous that the positive ions show maximum observed currents at zero $\Delta\phi$. The negative ions in fig. 3 end up on the nickel surface when $\Delta\phi$ is very positive; they accordingly are not detected. If $\Delta\phi << 0$ then the sampling cone strongly repels these negative ions, so they are again not detected, because few pass through the inlet orifice. In between these extremes, maximum currents are observed for negative ions (see fig. 3) when $\Delta\phi$ is in the range 0 to +5 V. These maximum currents are used when assessing the concentration of any ion in a flame.

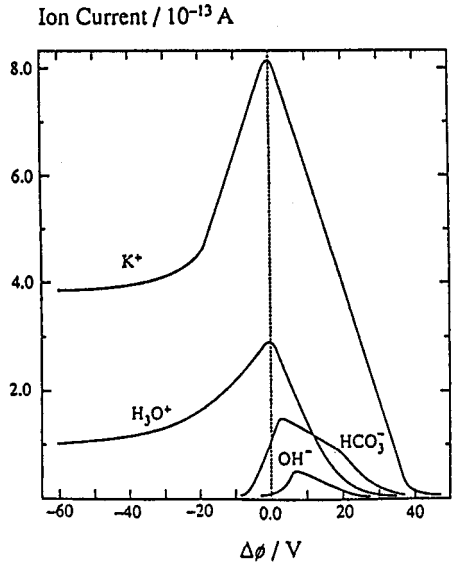

Fig. 3. Measured ion currents for the principal ions in a flame (unburnt composition: $H_2/O_2/N_2/CO_2$ = 1.50/1.00/4.67/0.38; final temperature = 1810 K) seeded with potassium. Observations were made 20 mm from the burner face. A positive $\Delta\phi$ means the sampling cone is at a positive potential with respect to the burner.

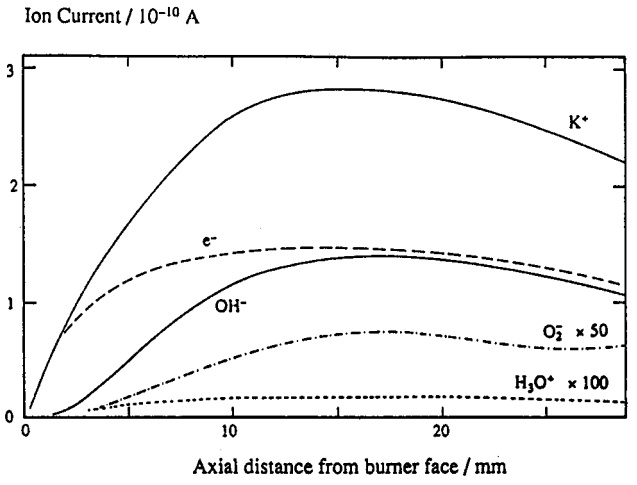

Fig. 4. Observed currents plotted against distance along the flame's axis. These observations are for M/10 KOH in the atomiser and a sampling hole 165 μm in diameter. For the sake of clarity some currents have been scaled by the factors shown.

NEGATIVE IONS (OH^- AND O_2^-) IN OXYGEN-RICH FLAMES

Initially, only one flame (see above) was investigated. Aqueous KOH was atomised into the gases supplied to the burner. In all, five sampling orifices were used with hole diameters of 60, 80, 115, 165 and 200 μm. If no solution was sprayed by the atomiser, no negative ions could be detected. A typical plot of all the ion-current profiles along the flame is shown in fig. 4. It can be seen that K^+ is the only significant positive ion observed here, although H_3O^+ is detectable at < 0.1% of the total positive ion current. The concentration of potassium ions rises rapidly to a broad maximum, where it remains fairly constant for several mm, but then begins to decrease at larger distances from the burner. The negative ions detected were OH^- and O_2^-, and, on occasion their hydrates, but these latter were always present at less than 1% of the relevant parent ion's concentration. It can be seen in fig. 4 that OH^- and O_2^- increase in concentration fairly slowly over the first few mm downstream from the burner, leading to reasonably constant levels for 20 or so mm, before being affected by cooling of the flame gases and air-entrainment. The electron concentration is also shown in fig. 4. It should be noted that the concentration of electrons can only be arrived at by an indirect method, since the mass spectrometer is not capable of detecting such a species with a very small mass to charge ratio. Therefore, given that charge neutrality must apply in the flame, the electron concentration is taken to be the difference between the total concentrations of all positive, $[P^+]$, and all negative ions $[N^-]$, *i.e.*

$$[e^-] = [P^+] - [N^-]$$

$$= [K^+] + [H_3O^+] - [OH^-] - [O_2^-]$$

The use of this method for determining electron concentrations may in itself produce odd results. It is known[9] that the errors associated with the sampling of positive ions are small, but as will be shown, sampling may well falsify, and thereby under-estimate the concentration of negative ion concentrations. In this case errors also arise in the electron concentration. Obviously, if $[P^+] >> [N^-]$, as is the case in many of the experiments described below, then $[e^-] \approx [P^+]$, and the errors in $[e^-]$ are probably unimportant. The following ratios: $[O_2^-]/[e^-]$, $[OH^-]/[O_2^-]$, and $[OH^-]/[e^-]$ were obtained from the ion current profiles in fig. 4 and are shown in fig. 5. In order to determine what the expected ion concentration ratios should be for thermodynamic equilibrium in a flame, the reactions

$$H_2O + e^- \rightleftharpoons H + OH^- \quad (+297 \text{ kJ/mol}) \quad (1)$$
$$HO_2 + e^- \rightleftharpoons H + O_2^- \quad (+147 \text{ kJ/mol}) \quad (2)$$
$$OH + e^- + M \rightleftharpoons OH^- + M \quad (-218 \text{ kJ/mol}) \quad (3)$$
$$O_2 + e^- + M \rightleftharpoons O_2^- + M \quad (-82 \text{ kJ/mol}) \quad (4)$$
$$O_2^- + OH \rightleftharpoons OH^- + O_2 \quad (-137 \text{ kJ/mol}) \quad (5)$$

were selected. The heats of reaction are quoted for a temperature of 2000 K and were derived from thermodynamic tables[10]. The forward and reverse rate coefficients of the i^{th} reaction are expressed as k_i and k_{-i}, respectively; the equilibrium constant will be written K_i. Thus we have:

$$\left(\frac{[OH^-]}{[e^-]}\right) = K_1 \left(\frac{p_{H_2O}}{p_H}\right)$$

where the equilibrium constant (of course, strictly dimensionless) has been expressed in effective units of partial pressure. Since, at early points in the burnt gases, the concentrations of OH and H radicals exceed[3] their final values for equilibrium, by the factors γ_{OH} and γ_H, respectively, the partial pressures of H and OH may be related to the relevant disequilibrium parameter by

$$p_{OH} = \gamma_{OH}.(x_{OH})_{final}.T/T_{final}.p_{total}$$
$$p_H = \gamma_H.(x_H)_{final}.T/T_{final}.p_{total}$$

where x_{OH} and x_H are the mole fractions of OH and H, respectively, the subscript *final* denotes the conditions that pertain to the gases well downstream of the burner, (T/T_{final}) is the ratio of burnt gas temperature at any particular point in a flame to the constant value which is ultimately reached downstream, and the total pressure, p_{total}, may be taken to be 1 atm.

When examining fig. 5 it is important to know what the values of $[OH^-]/[O_2^-]$, $[OH^-]/[e^-]$ and $[O_2^-]/[e^-]$ should be for thermodynamic equilibrium when $\gamma_{OH} = \gamma_H = \gamma_O = 1.0$, *i.e.* at around 20 mm downstream. The second column of Table 1 lists these values for conditions at 20 mm along the flame. The last column lists values for these three ratios for equilibrium in a sample originating from 20 mm downstream, but with

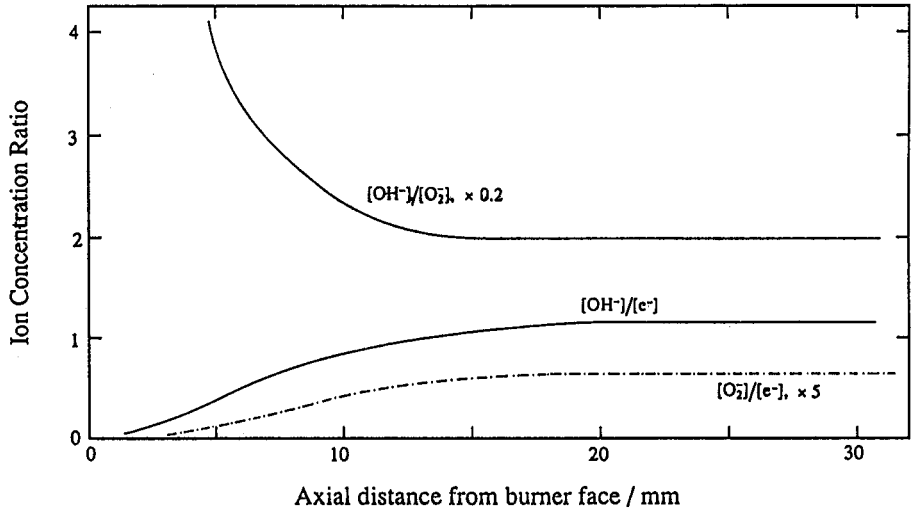

Fig. 5. Ratios of the principal negatively charged species, as derived from fig. 4. Some of the ratios have been scaled by the factors shown.

equilibrium maintained until conditions at the sampling nozzle's throat are reached. Thus the sample has been accelerated to a Mach number of unity, with the consequent cooling and fall in pressure, shifting these ratios. The discrepancies between measured and predicted ratios of ionic concentrations might be assumed to be caused by perturbations occurring during sampling. It is worth noting that both $[OH^-]/[O_2^-]$ and $[OH^-]/[e^-]$ increase threefold when the gas sample moves up to the throat of the inlet orifice. The result is that $[O_2^-]/[e^-]$ hardly changes. This is because the effects of a fall in temperature and pressure counteract one another. Such effects are now considered.

Table 1. Calculated ratios of concentrations of negatively-charged species at equilibrium

	Value for eq'm at 20 mm downstream in flame	Value for eq'm in sample from 20 mm, but at nozzles' throat
$[OH^-]/[O_2^-]$	24.8	63.2
$[OH^-]/[e^-]$	0.182	0.536
$[O_2^-]/[e^-]$	8.20×10^{-3}	8.42×10^{-3}

It was discussed above that an equilibrium such as (1) might shift position as the sample cools on entering the sampling system. Another important factor is that of loss of electrons from the gas during sampling. The extent to which this occurs is strongly related to the diameter of the sampling orifice and the level of ionisation within the flame. Greater electron loss is expected[9] when using a small hole, and also when there is less ionisation of the flame gases. Consideration of reactions (1) - (4) suggests that removal of electrons from the gas during sampling could bring about a shift in the equilibrium positions of these reactions. It should, perhaps, be noted at this point that a genuine loss of electrons will not necessarily be reflected in the derived electron concentration, $[e^-]$, this being the difference, $[P^+] - [N^-]$, discussed above. In fact, a loss of electrons may result in a concomitant loss of negative ions; if such a situation should arise, then the derived electron concentration, rather than falling, in line with the real concentration in the gas, will actually appear to increase. This effect may be of some consequence later. The present concern is simply whether a reaction will proceed and in which direction, and whether this will affect the measured concentrations. It is possible to calculate the concentrations of all the important neutral species, including the major radicals, in a flame as a function of distance from the reaction zone, and thus calculate the time constants for reactions (1) - (5). For this, it is necessary to take suitable values of rate coefficients and equilibrium constants for the above reactions. There is only slight uncertainty in the equilibrium constants, these being taken for the most part from the compilation of Jensen and Jones[11], or directly from thermodynamic tables[10]. However, there are errors associated with the rate coefficients. The literature has been searched and recommended rate coefficients are shown, together with the equilibrium constants for each reaction, in Table 2. The uncertainties in each of these rate coefficients are included in Table 2.

Table 2. Rate coefficients and equilibrium constants for reactions (1) - (5) (all are in the ml/molecule/s system of units.

Reaction	K_i	k_i	k_{-i}	Error factor in rate constants
(1)	$1600 \exp(-36060/T)$	$1.6 \times 10^{-6} \exp(-36060/T)$	1×10^{-9}	3
(2)	$1058 \exp(-18249/T)$	$2.12 \times 10^{-6} \exp(-18249/T)$	2×10^{-9}	3
(3)	$1.5 \times 10^{-22} \exp(24030/T)$	3×10^{-31}	$2 \times 10^{-9} \exp(-24030/T)$	10
(4)	$1.3 \times 10^{-21} \exp(7400/T)$	5×10^{-31}	$3.9 \times 10^{-10} \exp(-7400/T)$	5
(5)	$0.115 \exp(16630/T)$	1×10^{-10}	$8.7 \times 10^{-10} \exp(-16630/T)$	10

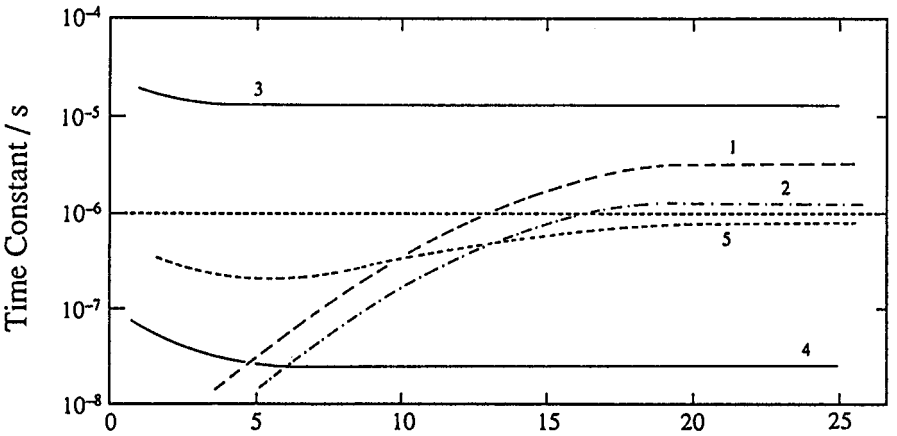

Fig. 6. Time constants for each reaction (as shown) at various points along the flame's axis.

The time constants τ for each of the above reactions have been calculated and are shown in fig. 6 as a function of distance along the flame. The line has been drawn, for τ = 1 μs, such that should the time constant for a reaction fall below this line, then it would be expected that that reaction might be perturbed during sampling, and as a consequence the composition altered. It is clear from fig. 6 that only reaction (3) is unaffected by sampling. However, every reaction appears to be equilibrated in this flame, in so far as every time constant is less than or equal to 10^{-5} s. In fact, for every reaction in all these flames, τ is maintained at approximately its flame value up to the throat of the sampling nozzle. From fig. 6 it is clear that reactions (4) and (5) alone are those that will undoubtedly be perturbed when sampling well downstream in the burnt gases. However, equilibria (1) and (2) will also be shifted, if the rate coefficients in Table 2 are correct, at points close to the burner, but not in those later parts of the burnt gases.

So far it has been established that the relaxation times for reactions (1) - (5) are all in the range 10^{-4} to 10^{-8} s. It is not possible for all the above reactions to be equilibrated simultaneously, because such a state of affairs would lead to conflicting results when the radical concentrations exceed unity, *i.e.* close to the burner. As an example, equilibration of (1) in isolation leads to $[OH^-]/[e^-] = K_1\,[H_2O]/\gamma_H[H]_{eq}$, whereas if only reaction (3) were balanced, then $[OH^-]/[e^-] = K_3\,\gamma_{OH}\,[OH]_{eq}$. These two results differ, if both γ_{OH} and γ_H exceed unity. On the other hand, these expressions for $[OH^-]/[e^-]$ equal one another if $\gamma_{OH} = \gamma_H = 1$. In such a situation, the pool of negatively charged species rapidly reaches a "steady-state" in a flame, whereby *e.g.* the rate of electron attachment to neutral species equals the rate of electron detachment. A steady state approximation on the electron concentration, *i.e.* $d[e^-]/dt \approx 0$, can be expressed as:

$$[e^-]\{k_1\,[H_2O] + k_2\,[HO_2] + k_3\,[OH][M] + k_4\,[O_2]\,[M]\} = [OH^-]\{k_{-1}\,[H] + k_{-2}\,[H][O_2^-]/[OH^-] + k_{-3}\,[M] + k_{-4}\,[M][O_2^-]/[OH^-]\}$$

Detailed examination shows that initially (at less than 9 mm above the burner) the first three terms on the left hand side are negligible. Also it is possible to conclude that, at closer than 4 mm from the burner's face, electron detachment is dominated by the reverse of reaction (1), when the above equation becomes

$$\frac{[OH^-]}{[e^-]} = \frac{k_4[O_2][M]}{k_{-1}\,[H]}$$

Of course, this ratio differs from that calculated by equating the forward and reverse steps of either reaction (1) or (3). However, at large times (at ≈ 20 mm) all the disequilibrium parameters become unity and $[OH^-]/[e^-]$ tends to the same value, as given by reaction (1) or (3) being at equilibrium. Thus, when γ_{OH}, γ_H and γ_O all become unity, reactions (1) and (3), if equilibrated, will predict identical $[OH^-]/[e^-]$.

Next the rates of production and disappearance of O_2^- ions can be equated, giving

$$\frac{[O_2^-]}{[e^-]} = \frac{k_4\,[O_2]\,[M]}{k_{-4}[M] + k_5[OH] + k_{-2}[H]}$$

for the first 4 mm. Clearly, early in a flame O_2^- is created by electron attachment to O_2. The rate of production of O_2^- equals the rate at which O_2^- transfers an electron to OH, or detaches an electron in

colliding with M or H.The above ratios have been derived for the first 4 mm of the burnt gases and lead to:

$$\frac{[OH^-]}{[O_2^-]} = \frac{k_{-4}[M] + k_5[OH] + k_{-2}[H]}{k_{-1}[H]}$$

Other relations could be derived from the steady state equations for the other parts of the flame. However, it is of interest to compare the above simple ratios with those obtained from assuming reactions (3) and (4) are separately and independently equilibrated early in a flame.

THE RATIO $[O_2^-]/[e^-]$

Figure 7 shows the measured ratio $[O_2^-]/[e^-]$ plotted logarithmically as a function of distance from the burner, for three molarities of KOH (graphs (a), (b) and (c)), and sampling with five orifices. Also shown in fig. 7 is the predicted steady-state value of $[O_2^-]/[e^-]$ very early and also the equilibrium value late in the flame. Initially, the region of the flame where all reactions should be equilibrated will be considered. Fig. 7(a) shows that over the range z = 20 - 30 mm, $[O_2^-]/[e^-]$ is virtually constant, and of similar magnitude for all holes, except with the smallest (diam. 60 μm). The results presented in fig. 7(a) with the 165 μm orifice must be considered erroneous, since the large $[O_2^-]/[e^-]$ seen here are not observed in fig. 7(b and c). It can be seen in fig. 7(a), that the larger holes give $[O_2^-]/[e^-]$ greater than that predicted

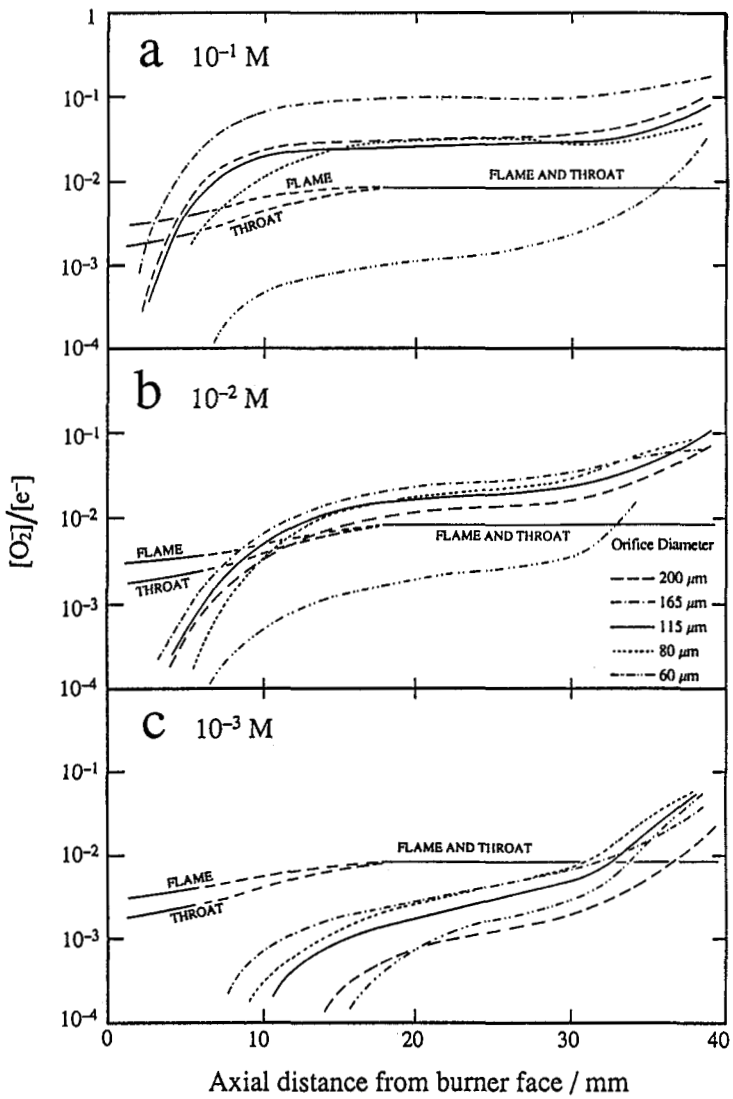

Fig. 7. Measured profiles of $[O_2^-]/[e^-]$ in the flame. The orifice diameters and molarities of KOH sprayed in the atomiser are as indicated. Also the steady state predictions are shown.

for equilibrium, whereas the smallest has $[O_2^-]/[e^-]$ much lower. It is necessary to consider here the rôle of two possible sampling perturbations. The first is cooling of the gas sample in the thermal boundary layers, this cooling being additional to the aerodynamic cooling always experienced for an acceleration to a Mach number of unity. The second perturbation derives from the effect of electron loss on those gases close to the sampling nozzle. It was noted above that only reactions (4) and (5) have time constants small enough to allow their equilibria to be shifted during sampling of the gases well downstream. The behaviour of (4) and (5) in this region of the burnt gases will now be investigated in detail. Noting first that $[O_2^-]/[e^-]$ is found to be above its equilibrium level in the later parts of the burnt gases, the implication of this is that cooling has occurred to the gas during sampling. However, Table 1 indicates that $[O_2^-]/[e^-]$ at the throat should be similar to that in the flame. If, though, a significant amount of boundary layer cooling has occurred, $[O_2^-]/[e^-]$ will have increased as a result of reaction (4) moving in the exothermic direction. The increase in $[O_2^-]/[e^-]$ is by a factor of ~3, which implies, from a consideration of the exothermicity of reaction (4), that cooling of some 380 K in the boundary layer, in addition to the subsequent aerodynamic cooling, must have occurred. For a flame of similar temperature, Burdett and Hayhurst[6] calculated the mean cooling in the boundary layer of an orifice of diameter 200 μm as around 310 K. These two falls in temperature are in reasonable agreement, and give a satisfactory explanation for the high level of $[O_2^-]/[e^-]$ seen in fig. 7(a), when sampling with the largest orifice. Of course, the effect of boundary layer cooling should be greater as the orifice size is reduced, and this is not immediately apparent in fig. 7(a). As a consequence, it is necessary to consider the likely effect on $[O_2^-]/[e^-]$ of losing electrons from the burnt gases by *e.g.* diffusion to the sampling nozzle. A loss of electrons will tend to force reaction (4) to move in the reverse direction, reducing the concentration of O_2^- in the sample, and leading to a lowering of $[O_2^-]/[e^-]$. The observed ratio $[O_2^-]/[e^-]$ is lowered, because the derived $[e^-]$ is effectively determined by the concentration of positive ions in the flame; a real loss of electrons will not affect the derived electron concentration to any significant extent. Thus, $[O_2^-]/[e^-]$ falls as electrons are lost, because $[O_2^-]$ is reduced through the action of *e.g.* reaction (4), but $[e^-]$ remains unaltered. This effect will occur to a greater extent with smaller holes, and particularly at lower levels of ionisation in the flame, as in the plots shown in fig. 7(b and c). Considering first the case of the smallest orifice, fig. 7(a) shows that $[O_2^-]/[e^-]$ is much lower than expected, and, in fact, a similar $[O_2^-]/[e^-]$ is observed in fig. 7(b and c), to within one order of magnitude. This observation must be ascribed to electron loss. The result is to lower $[O_2^-]/[e^-]$ significantly for the small orifice, but to a far lesser extent with the bigger holes. Such a state of affairs would, however, enable the lack of any systematic trend in $[O_2^-]/[e^-]$ with hole size, for the 80-165 μm orifices, to be explained. In other words, with a medium-sized orifice, the boundary layer cooling would be expected to give $[O_2^-]/[e^-]$ greater than with the 200 μm hole, but the increased electron loss experienced with the former will reduce $[O_2^-]/[e^-]$, so that the observed $[O_2^-]/[e^-]$ are comparable in all cases, except that of the tiniest hole.

If fig. 7(b and c) is now considered, it is seen that there is a reduction in $[O_2^-]/[e^-]$ as the molarity of KOH is lowered. This occurs with all holes, except the smallest, which has a reasonably constant $[O_2^-]/[e^-]$ as the molarity changes. Once again, loss of electrons, which occurs to a greater extent at low levels of ionisation in a flame, may be invoked to explain the observations. As the electron concentration falls during sampling, reaction (4) shifts extremely rapidly (see fig. 6) so that O_2^- is removed from the gas. This clearly happens to a more significant extent at low molarity, as may be seen in fig. 7. In fact, fig. 7(c) does show some dependence of $[O_2^-]/[e^-]$ on hole size, $[O_2^-]/[e^-]$ being smallest for the 200 and 60 μm, and largest for the medium-sized, orifices. This observation may be explained by considering the opposing effects of cooling and electron loss on $[O_2^-]/[e^-]$ at different orifice diameters. For a large hole, the increase in $[O_2^-]/[e^-]$ by cooling is small, but the reduction due to electron loss may be important at such a low molarity. In contrast, for a small hole, the increase in $[O_2^-]/[e^-]$ by cooling will be large, but the reduction in $[O_2^-]/[e^-]$ will also be greater than with a big hole. Thus for these extremes of orifice diameter, similar, and low, values of $[O_2^-]/[e^-]$ are seen. With a medium-sized hole, the increase in $[O_2^-]/[e^-]$ will be more significant than when sampling through the largest orifice, but the amount of electron loss may not be substantially more. Therefore, $[O_2^-]/[e^-]$ is found to be slightly greater than with either a very small or a very large orifice. In relation to all of the above discussion, the role of reaction (5) must not be ignored, since it has a time constant which permits perturbation of (5) by sampling. As a consequence, cooling will result in the removal of O_2^- to form OH^-, but if $[O_2^-]$ is reduced on account of electron loss, then (5) will form O_2^- from OH^-, provided the reduction in $[O_2^-]$ is significant enough to prevent (5) moving in the exothermic direction as the gases are cooled.

Turning now to the early parts of the flame, fig. 7(a) shows that reasonably good agreement is found between the observed $[O_2^-]/[e^-]$, and those predicted from the steady state. It is apparent that sampling perturbations exist in this region of the flame, from a comparison of the plots in (a), (b) and (c) of fig. 7. In fig. 7(a), although $[O_2^-]/[e^-]$ is close to the predicted value, in fact, the observed initial $[O_2^-]/[e^-]$ are lower than expected. Then immediately downstream (for z = 5 - 15 mm), with all but the smallest holes, the situation reverses to the observed values exceeding the computed ones. Fig. 6 shows that reactions (1) and (2) may now be affected by sampling, so that nearer the burner, (2) will remove O_2^- if the sample is cooled or if electron loss occurs. In fact, reaction (2) is now the principal route for the loss of O_2^-, since the response of (2) to changes in temperature and electron concentration will be more rapid than reaction (4), when sampling close to the burner. It may be noticed from fig. 7(b and c), that at low molarities of KOH, few points are shown in the steady state region, for the simple reason that the ion currents due to OH^- and O_2^- were too small to be measured in this part of the flame. It is clear from a comparison of (a), (b) and (c) in fig. 7 that the effects of cooling and electron loss still apply to those regions of the flame where not all reactions are expected yet to be fully equilibrated, *i.e.* for z = 5 - 15 mm. The lowering of $[O_2^-]/[e^-]$ seen in fig. 7(a), near the burner, may be caused by reaction (2) proceeding during sampling for longer than any of the others. In this way a sampling perturbation can arise, even though $[O_2^-]/[e^-]$ is governed by a steady state rule.

One final feature of interest is the increase in O_2^- seen at z = 30 mm in fig. 7. This is caused by air-entrainment, and the effects of drawing air from the laboratory into the flame are to cool the gases, and to increase the amount of O_2 present. Thus, reaction (4) will form significant quantities of O_2^- as a result of increased electron attachment in (4). The increase in $[O_2^-]$ begins at around 30 mm from the burner, and clearly illustrates the relatively short distance, compared with a fuel-rich flame, over which sampling from an oxygen-rich flame may be made without disruption from laboratory air.

CONCLUSION

The general principles whereby the composition of a sample can be perturbed during sampling have been explored. The rate constants chosen in Table 1 seem to be fairly accurate at explaining the observations, particularly when the ratios $[OH^-]/[O_2^-]$ and $[OH^-]/[e^-]$ are explored in detail[12]. Perhaps a novelty in this study arises from perturbations caused by electrons diffusing to the metallic sampling nozzle.

REFERENCES

1. O.P. Korobeinichev, Uspekhi Khimii, 49, 945-965 (1980).
2. A.N. Hayhurst, Bull. Soc. Chim. Belg., 99, 451-459 (1990).
3. J.M. Goodings and A.N. Hayhurst, J. Chem. Soc., Faraday Trans. 2, 84, 745-762 (1988).
4. J.M. Kay and R.M. Nedderman, Fluid Mechanics and Transfer Processes, Cambridge University Press, 1985.
5. A.N. Hayhurst and N.R. Telford, Combustion and Flame, 28, 67-80 (1977).
6. N.A. Burdett and A.N. Hayhurst, J. Chem. Soc., Faraday Trans. 1, 78, 2997-3007 (1982).
7. A.N. Hayhurst and N.R. Telford, Proc. Roy. Soc. Lond. A., 322, 483-507 (1971).
8. N.A. Burdett and A.N. Hayhurst, Proc. Roy. Soc. Lond. A., 355, 377-405 (1977).
9. S.D.T. Axford and A.N. Hayhurst, Int. J. Mass Spec. and Ion. Proc., 110, 31-65 (1991).
10. JANAF Thermodynamic Tables, N.B.S., 1985.
11. D.E. Jensen and G.A. Jones, Combustion and Flame, 32, 1-32 (1978).
12. S.D.T. Axford and A.N. Hayhurst, to be published.